Geomechanics and Engineering, *Vol. 29, No. 1 (2022) 91-97*
https://doi.org/10.12989/gae.2022.29.1.091

Model tests for the inhibition effects of cohesive non-swelling soil layer on expansive soil

Zheng Lu[1,2], Chuxuan Tang*[1,3], Hailin Yao[1], Jianbo She[4], Ming Cheng[5], Yu Qiu[1,3] and Yang Zhao[1,3]

[1]*State Key Laboratory of Geomechanics and Geotechnical Engineering, Institute of Rock and Soil Mechanics, Chinese Academy of Sciences, Wuhan 430071, People's Republic of China*
[2]*Hubei Key Laboratory of Geo-Environmental Engineering, Wuhan 430071, People's Republic of China*
[3]*University of Chinese Academy of Sciences, Beijing 100049, People's Republic of China*
[4]*Jinke property group Hubei Co. Ltd, Wuhan 430063, People's Republic of China*
[5]*Jilin Provincial Transport Scientific Research Institute, Changchun 130012, People's Republic of China*

(Received October 26, 2021, Revised February 16 2022, Accepted February 22, 2022)

Abstract. The cohesive non-swelling soil (CNS) cushion technology has been widely applied in the subgrade and slope improvement at expansive soil regions. However, the mechanism of the inhibition effect of the CNS layer on expansive soil (ES) has not been fully understood. We performed four outdoor model tests to further understand the inhibition effect, including different kinds of upper layer and thickness, under the unidirectional seepage condition. The swelling deformation, soil pressure, and electrical resistivity were constantly monitored during the saturation process. It is found that when a CNS layer covered the ES layer, the swelling deformation and electrical resistivity of the ES layer decreased significantly, especially the upper part. The inhibition effect of the CNS layer increases with the increase of CNS thickness. The distribution of vertical and lateral soil pressure also changed with the covering of a CNS layer. The electrical resistivity can be an effective index to describe the swelling deformation of ES layer and analyze the inhibition effect of the CNS layer. Overall, the CNS deadweight and the ion migration are the major factors that inhibit the swelling deformation of expansive soil.

Keywords: cohesive non-expansive soil; electrical resistivity; expansive soil; model test; soil pressure; swelling deformation

1. Introduction

Expansive soil, which has characteristics of water swelling and drying shrinkage, is widely distributed around the world (Ali *et al.* 2020, Bowels 1988, Jones and Jefferson 2012). The swelling and drying behavior of expansive soil causes huge damage to the geotechnical structures, including road subgrade and slope (Chompoorat *et al.* 2021, Nalbantoğlu 2004, Punthutaecha *et al.* 2006) . Therefore, controlling the swelling and shrinkage deformation of expansive soil is vital to the safety and stability of engineering structures (Cheng *et al.* 2018, Puppala *et al.* 2005).

To eliminate or inhibit the swell-shrink behavior of expansive soil (ES), many researchers have applied the cohesive non-swelling soil (CNS) covering technology for its reliability and efficiency (Chen *et al.* 2006, Katti 1979, Murty and Praveen 2008, S9451 1994, Watanabe *et al.* 2021). However, the interaction between CNS layer and ES layer has not been fully understood. It is generally accepted that the CNS layer can protect the ES layer from the variation of water and heat induced by the natural environment, and the deadweight of CNS layer can also inhibit the swelling deformation of ES layer. Katti *et al.* (2002) found that the expansion of the black cotton soil can be eliminated with 1.2 m CNS covered even when subjected to infiltration saturation. Although the deadweight of the CNS layer can contribute to the inhibition of soil expansion, the deadweight is much lower than the swelling pressure (224 kPa). Therefore, there should exist other interactions between the CNS layer and the ES layer except for the deadweight. Yao *et al.* (2020) performed laboratory tests to study the effects of CNS layers. They found that ions in the CNS layer would migrate and concentrate in the ES layer during a unidirectional saturation, and the inhibition effects of migrated ions are more significant than the effects of CNS deadweight. However, their conclusion is limited by the model size that is much smaller than the actual size. Compared to filed and laboratory tests, the outdoor model test is more suitable for controlling the boundary condition of tests and simulating the actual situation as real as possible.

During the infiltration saturation test, the soil expansion happens in a water-ion-soil system, where the increase of water content, migration of ions, and soil deformation simultaneously occur. It is actually an electrochemistry process. In the conventional tests, only mechanical indexes, including swelling deformation and soil pressure, are tested. The electrical resistivity is sensitive to the composition and structural characteristics of soil (Lei *et al.* 2021, Oh *et al.*

*Corresponding author, Ph.D.
E-mail: tangchuxuan18@mails.ucas.ac.cn

ISSN: 2005-307X (Print), 2092-6219 (Online)

2015). Since Archie (1942) first proposed the formula for saturated sand resistivity, researchers have performed many tests to study the influence of parameters, including water content, temperature (AbuHassanein *et al.* 1996), and other geotechnical factors (Kibria and Hossain 2012) on the electrical resistivity of clays. Cai *et al.* (2015) performed systematic experiments to study the correlation between the electrical resistivity, and mechanical properties of MgO stabilized silty soil. Chu *et al.* (2018) found that it is practical to predict the free swelling rate of expansive soil using the electrical response. From the listed literature, we can infer that the electrical resistivity can be applied to study the mechanism of inhibition effects of CNS layer on ES layer.

In this paper, we performed four outdoor model tests to study the inhibition effect of CNS layer with different thicknesses on ES layer under unidirectional saturation. During the saturation process, the electrical resistivity, swelling deformation, soil pressure were continually monitored to analyze the inhibition effect of CNS layer on ES layer.

2. Model description

2.1 Physical parameters of test soil samples

The expansive soil adopted in this test was obtained from Nanning, Guangxi province, China. The CNS was obtained from Wuhan, Hubei province, China. The physical parameters of the soils are shown in Table 1. Katti *et al*. (2002) proposed tentative specifications for CNS soils, as shown in Table 2. Indeed, the soil as shown in Table 1 does not satisfy the recommended requirements in Table 2. However, this soil has been used as CNS material for a series of small model tests (Yao *et al*. 2020), and they found that this soil can significantly restrain the swelling characteristics of expansive soil. Therefore, the soil as shown in Table 1 can be applied as CNS material and be used to study the effects of cohesive non-swelling soil layer on expansive soil.

Table 1 Physical properties of soils

Index	CNS	Expensive soil
Sand (%)	1.40	3.90
Silt (%)	64.20	31.70
Clay (%)	34.40	64.40
Specific gravity	2.73	2.70
Liquid limit (%)	37.23	63.00
Plastic limit (%)	20.10	24.94
Unified soil classification	CL	CH
Optimum moisture content (%)	13.80	16.20
Maximum dry density (g/cm^3)	1.92	1.80
Free swelling ratio (%)	24.50	65.50
Swelling force (kPa)	--	182.72
Swelling percentage (%)	--	19
Permeability (cm/s)	2.87×10^{-7}	4.86×10^{-8}

Table 2 Physical properties of CNS soil (Katti *et al.* 2002)

Clay (less than 2 μm)	15–20%
Slit (0.06 mm–0.002 mm)	30–40%
Sand (2 mm–0.06 mm)	30–40%
Gravel (Greater than 2 mm)	0–10%
Liquid limit	30%- 50%
Plasticity index	15%- 30%

2.2 Model design

As shown in Fig. 1, the dimensions of the test box are 2.4 m ×1.8 m × 2.8 m (height). Most parts of the box were buried, and 0.5 m of the box extended out of the ground to prevent water in surrounding soils from entering. The one-time-forming test box was made of steel-reinforced concrete to ensure enough rigidity, and it was partitioned into six cells with a size of 40 cm × 40 cm by the inner wall. Different kinds of models were filled in the cells, as shown in Fig. 1(b). The walls in each cell were paved with an asphalt waterproofing membrane to prevent water penetration and reduce friction between soil and wall. Silicone oil was also put on the membrane surface to reduce friction. One side of each model was blocked by the organic glass plates with a thickness of 10 mm for observation, as shown in Fig. 1(a). The plates were fixed to the sidewall by corner connectors, bolts, and rivets. We applied several waterproof measures to prevent water leaking from the gap between the organic glass plate and the wall. Besides, the outside of glass plates was supported by steel transverse braces at certain intervals to limit lateral deformation of models during the test. According to the real working condition, a certain thickness of expansive soil was first filled, followed by another layer of CNS. In addition, the infiltration of water was simplified to the unidirectional seepage condition, where the distilled water was injected on the top surface of models, as shown in Fig. 1(b).

2.3 Experimental plan

To study the inhibition effect of CNS on expansive soil, we designed 4 kinds of models with the same thickness of ES (60 cm) and different upper layers, as shown in Table 3. The effects of CNS thickness were studied by setting three kinds of thickness, including 0, 40, and 80 cm. In addition, a control experiment (test 4), which contained a layer of gravel with the same weight of 40 cm CNS layer, was also performed to discuss the effects of upper layer deadweight separately. It needs to be pointed out that the gravel had been washed many times to ensure that the deadweight of gravel is the only influence factor on the swelling deformation of the expansive soil layer. Several indexes, including swelling deformation, electrical resistivity, and soil pressure, were monitored during water infiltration.

2.4 Monitoring method

To monitor the variation of indexes, as shown in Table 3, several devices and sensors are needed to be buried during the filling of models.

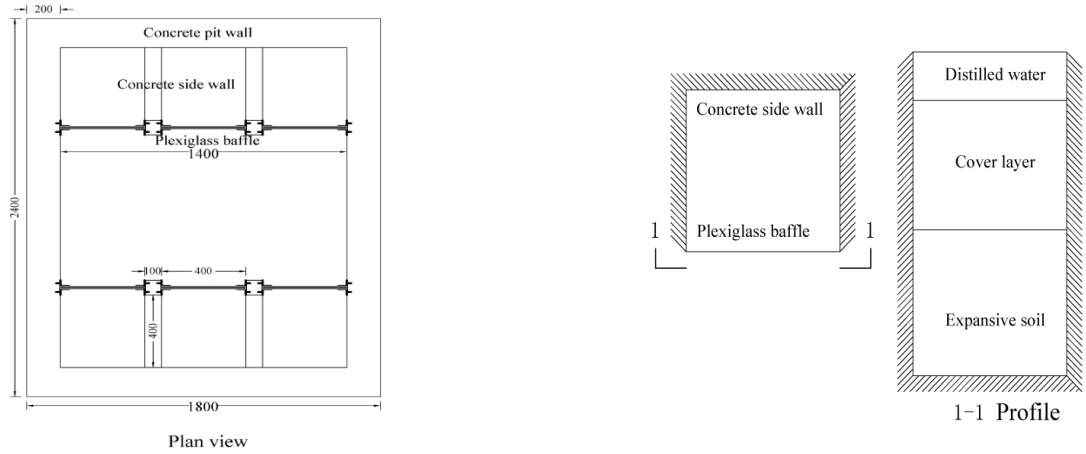

(a) Plan of the model test tank (mm) (b) Diagram of a test cell

Fig. 1 Design of the model test

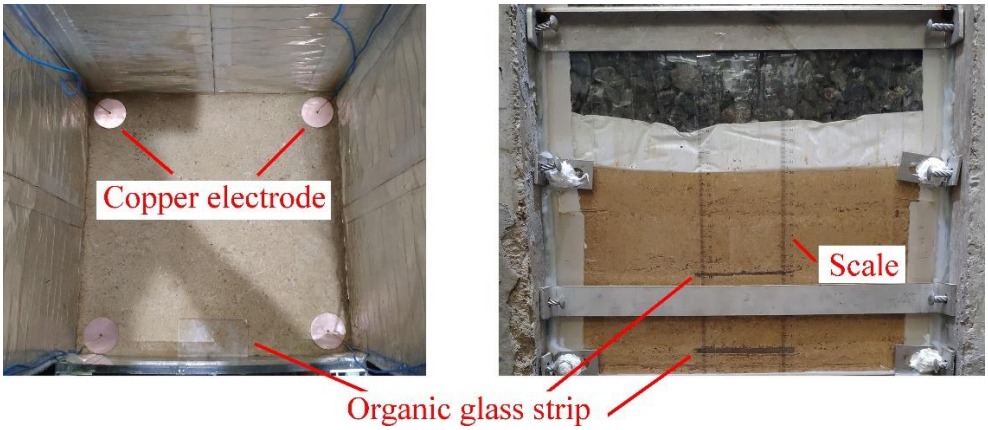

Fig. 2 Placement of organic glass strip and copper electrode

Table 3 Outdoor model test plan

Number	Model type	ES thickness /cm	Cover layer thickness /cm	Type of cover layer	Soil compactness /%	Monitor parameters
1	ES 60+CNS 0	60	0	——	85	Swelling deformation, electrical resistivity, soil pressure
2	ES 60+CNS 40	60	40	CNS	85	
3	ES 60+CNS 80	60	80	CNS	85	
4	ES 60+Gravel 40	60	——	Gravel	85	

2.4.1 Swelling deformation

As shown in Fig. 2, organic glass strips with a size of 10 cm × 5 cm were placed beside the organic glass plate for every 10 cm thickness of expansive soil during model filling. When the expansive soil swells in the saturation process, the strips will move with the soil, the moving distance of which can be observed according to the scales on the plate, as shown in Fig. 2. Therefore, by constantly recording the movement of strips at different depths, the swelling deformation of different expansive soil layers can be obtained.

2.4.2 Electrical resistivity

To test the electrical resistivity of the expansive soil layer during the saturation process, we installed copper electrodes in the bottom, middle, and top of the expansive soil layer, as shown in Fig. 2. The diameter and thickness of the round copper electrode is respectively 5 cm and 1 mm. Through the 2 mm hole in the center of the electrode, a wire was tied to the electrode and extended out of the box for testing convenience. Because the electrical resistivity is associated with temperature (AbuHassanein *et al.* 1996), we measured the electrical resistivity of models at a fixed time in the evening to deduce the influence of temperature.

The electrical resistivity of the bottom and the upper half of the expansive soil layer were tested by the Pentium WDJD-4 digital DC electronic activator with a DC power supply, as shown in Fig. 3. The electrical resistivity of the tested layer can be obtained by the following expression

$$\rho = \frac{(\Delta U - \Delta U_{sp})S}{IL} \quad (1)$$

where ΔU and ΔU_{sp} are respectively the measured and original potential difference of the tested soil layer; I is the current size; L is the thickness of the soil layer; S is the area of the round copper electrode.

2.4.3 Soil pressure

For tests 1-3, the vertical and transverse soil pressure was recorded using soil pressure sensors. The thickness of the soil pressure sensor is 2 cm and the diameter of it is 10 cm. Before the filling of ES layer, one soil pressure sensor was set horizontally at the center of the box bottom, and another soil pressure sensor was set vertically next to the concrete wall. When the height of ES layer respectively reaches 30 and 60 cm, two soil pressure sensors were also installed at the bottom of the box. Therefore, the vertical and transverse soil pressure in the bottom, medium, and top of the expansive soil layer can be recorded during the saturation process.

The data of the soil pressure sensor with 2 cm thickness and 10 cm diameter were collected by the UT7110Y static strain gauge, the accuracy of which is 0.01 kPa.

2.5 Model filling

The bulk soil was first subjected to air-drying, crushing, and processing through a 2.00 mm sieve. Then, an amount of water was sprayed on the soil powder to reach the optimum water content, and the soil sample was ready to be filled after storage in an airtight container for 4 days. Considering the amount of soil needed for this experiment is large, we prepared the soil for each model individually, and the water content is tested before the filling of models.

The initial water content of each model is listed in Table 4. As shown in Table 4, the water content of the soil is controlled well in the range of ±0.5% around the optimum water content. To accelerate the infiltration process, we set the degree of soil compaction to 85%. Referring to the scale on the organic glass plate, we compacted the soil at layers every 5 cm. As described in the above sections, the devices and sensors were buried in a specific depth during the filling process. After the filling of the model, one layer of filter paper and geotextile was placed on the top surface of the soil, and then 3 kg gravel was uniformly distributed on the geotextile to reduce the disturbance to the surface soil when adding water. Finally, distilled water was added to the model after recording the initial values of electrical resistivity and soil pressure. In addition, the thickness of water was kept around 5 cm during the whole saturation process.

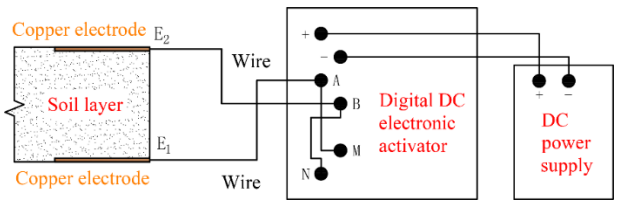

Fig. 3 Measurement of electrical resistivity

Table 4 Initial water content of soil for each model

Soil type	Water content (%)			
	ES 60+CNS 0	ES 60+CNS 40	ES 60+CNS 80	ES 60+Gravel 40
CNS	-	13.56	14.31	-
Expensive Soil	16.10	15.83	16.44	16.34

3. Results analysis

3.1 Swelling deformation

The developments of swelling deformation for the 60 cm expansive soil layer in different tests are shown in Fig. 4. As can be found, the swelling deformation of the model without the CNS layer continued to grow with time and finally reached 41.5 mm. When the ES layer was covered with a 40 cm thick CNS layer, the stable swelling deformation was reduced to 13 mm, and the inhibition ratio reaches 68.67%. The inhibition effect increased with the increase of CNS thickness, and the swelling deformation of ES layer was only 4.5 mm as the thickness of CNS increased to 80 mm. However, when the 40 cm thick CNS layer was replaced by an equal weight of gravel, the inhibition ratio was only 48.2%, which is much lower than the effect of 40 cm thick CNS layer. This indicates that there must exist other effects of the CNS layer on the swelling behavior of ES layer besides the effect of CNS deadweight.

Fig. 5 respectively shows the swelling deformation of six layers with the same original thickness in the ES. It can be found that the swelling deformation mainly formed in the upper part of the ES layer (30-60 cm) for the models without a CNS layer. Without a covering layer (ES 60+CNS 0), the swelling deformation for the upper layer of ES was 29.5 mm, which accounted for 71% of the whole swelling deformation. When covered with a gravel layer, the swelling deformation for all layers shows a certain decrease.

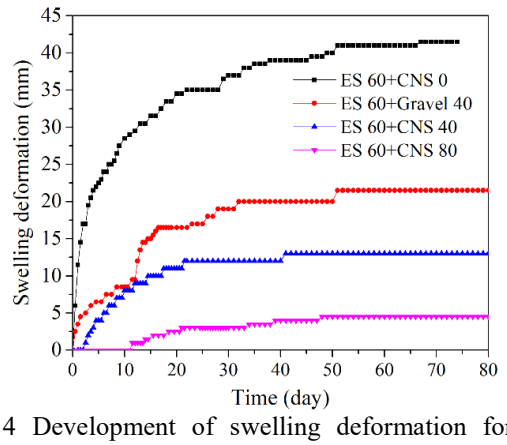

Fig. 4 Development of swelling deformation for the whole expansive soil layer

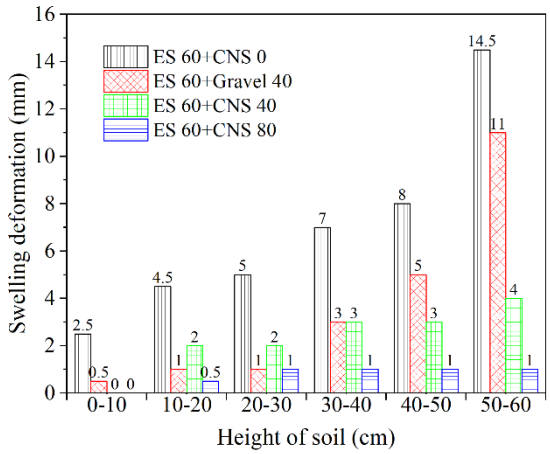

Fig. 5 Stable swelling deformation of the expansive soil in the different height range

Further, the swelling deformation of the ES upper part decreased significantly with the covering of CNS layer, while the variation of swelling deformation in the lower part was not obvious. This means that the inhibition effect (exclude the effect of CNS deadweight) of the CNS layer on the ES layer is mainly concentrated on the upper part of ES layer.

3.2 Electrical resistivity

As described in 2.4.2, copper electrodes were installed in the bottom, middle, and top of the ES layer. With the buried electrodes, the electrical resistivity of the lower part (0-30 cm) and the upper part (30-60 cm) of the ES layer were monitored constantly during the saturation process, as shown in Figs. 6(a) and 6(b). It needs to be pointed out that we monitored the electrical resistivity of a specific soil layer at 4 corners, corresponding to 4 copper electrodes in Fig. 2, and the consistency of test results for the 4 groups is high. Therefore, to ensure the clarity of figures, we only present the mean values of the 4 groups of data. As shown in Fig. 6(a), the initial electrical resistivity of the lower part is different for different models. This phenomenon can be attributed to the different water contents of each model before the saturation process (see Table 4). The pore water of CNS layer can seep into the ES layer, which leads to the decrease of initial electrical resistivity of the upper layer (Fig. 6(b)). This is the reason why the initial electrical resistivity of the upper part is much lower than that of the lower part for ES 60 + CNS 40 and ES 60 + CNS 80. When the distilled water was added to the top of the models, the water gradually seeped into the soils, leading to a significant decrease in electrical resistivity. The decrease of electrical resistivity happened immediately for the upper part of the ES layer, and then gradually reached an equilibrium state. As for the electrical resistivity of the ES lower part, it was stable at the beginning because it cost days for the water to seep into the lower part.

The final stable values of all the four tests are summarized and shown in Fig. 7. It can be found that the electrical resistivity of the upper part was a little lower than that of the lower part for the models without a cover layer.

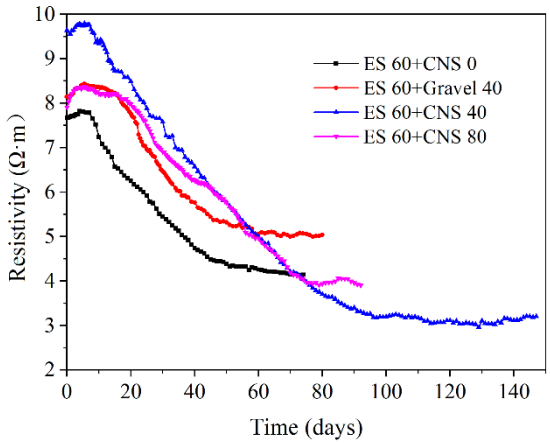

(a) Lower part

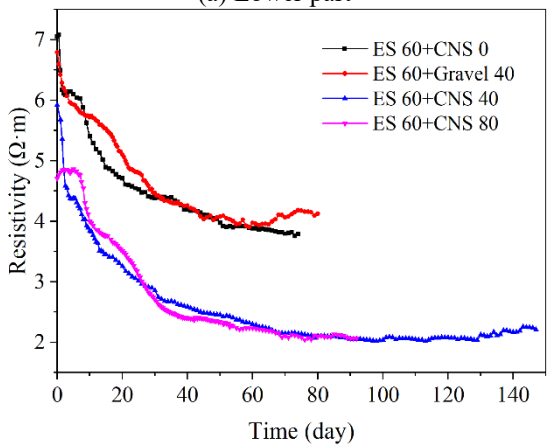

(b) Upper part

Fig. 6 The variation of electrical resistivity for different parts of the expansive soil

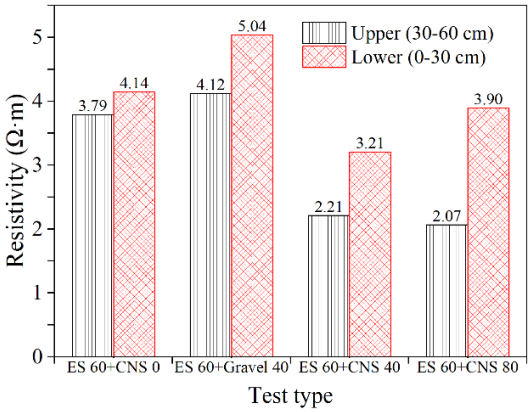

Fig. 7 Comparison of stable electrical resistivity for different parts of the expansive soil layer

This is because the swelling deformation of ES upper part was larger than the lower part, as shown in Fig. 5, leading to a larger pore ratio and lower electrical resistivity. When the ES layer was covered by a layer of gravel, the swelling deformation was decreased, and the electrical resistivity of both layers increased, as shown in Fig. 7. However, although the swelling deformation decreased when the ES layer was covered by a CNS layer, the electrical resistivity of both ES layers showed a significant decrease. This can be attributed to the ion migration from the CNS layer to the

ES layer during the saturation process, which has been proved in the laboratory test in Yao *et al*. (2020). It needs to be pointed out that the electrical resistivity of the lower part for ES 60+CNS 40 was slightly lower than that for ES 60+CNS 0, but the electrical resistivity of the upper part decreased around 50% when a 40 cm CNS layer covered the ES layer. This implies that the ions migrated from the upper layer mainly concentrated on the upper part of the ES layer.

3.3 Soil pressure

Fig. 8 presents the stable soil pressure at the bottom, middle and top of the ES layer in both the vertical and lateral directions. From Fig. 8(a), it can be found that the vertical soil pressure was the largest at the bottom of ES layer for ES 60+CNS 0, and the vertical soil pressure decreased significantly at higher places. This is because the swelling deformation was larger as height increases, and the swelling pressure was released during the swelling deformation. However, the vertical pressure at all the three layers was almost equal for the other two models, and even the swelling deformation was much lower. This phenomenon means that the expansibility of ES soils was inhibited because of the CNS layer. Yao *et al.* (2020) tested the expansibilities of ES soil after a similar saturation process in the laboratory model test. And they found that the swelling percentage and swelling force of expansive soil decreased significantly after tests because of the ion migration from the CNS layer during the saturation process. As shown in Fig. 8(b), the lateral soil pressure for the three layers were almost the same because the lateral deformation was limited. When the ES layer was covered with a 40 cm CNS layer, the lateral soil pressure slightly decreased because of the inhibition effect of migrated ions. However, the lateral soil pressure significantly increased when covered with an 80 cm CNS layer and was close to the vertical soil pressure because the 80 cm CNS layer significantly limited the deformation of ES layer.

3.4 Soil properties

After the tests, soil samples were obtained in the ES layer for every 20 cm. The moisture content and compactness of soils along the height were tested through the samples and shown in Fig. 9. The ES soils were all saturated after tests, and the variations of moisture content and compactness were corresponding to the different swelling deformation (Fig. 5). As shown in Fig. 9(a), the soil moisture content was the largest at the top and gradually decreased at deeper places, which was similar to the variation of vertical deformation. Contrary to the variation of vertical deformation, the soil compactness increased in a deeper place (Fig. 9(b)). The variations of soil compactness of ES 60+CNS 0 and ES 60+Gravel 40 along the soil height were high. However, the soil compactness became stable along with the height when covered with the CNS layer, and the distribution of soil compactness gradually get closer to the original state with a thicker CNS layer.

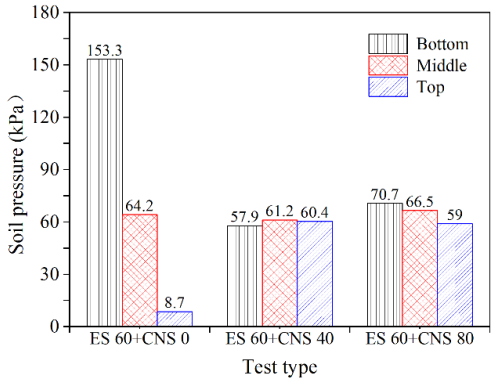

(a) Vertical

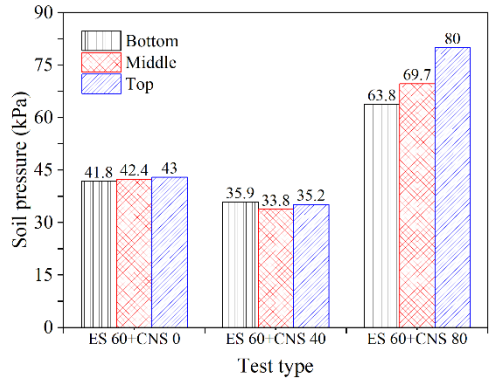

(b) Lateral

Fig. 8 Stable soil pressure for different parts of the ES layer in different directions

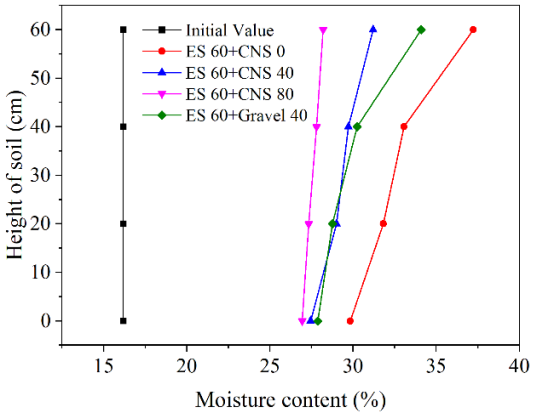

(a) Moisture content

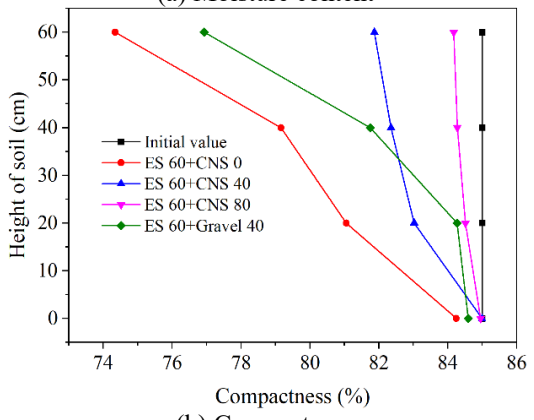

(b) Compactness

Fig. 9 Variation of soil properties along with the height of expansive soil after the experiment

4. Conclusions

To study the inhibition effect of the CNS layer on the ES layer, we monitored the swelling deformation, electrical resistivity, soil pressure of different layers inside the ES layers of four different models during the unidirectional saturation. The following conclusions can be obtained:

• The CNS layer can significantly inhibit the swelling deformation of ES layer, and the inhibition effect increases with the increase of CNS thickness.

• During the saturation process, ions of the CNS layer migrate into the ES layer, leading to a significant decrease in electrical resistivity of the ES layer, especially the upper part. The migrated ions can decrease the swelling deformation and soil pressure of the ES layer.

• The gravel layer can only physically inhibit the swelling deformation of ES layer by its deadweight without electrochemical effects.

• The CNS layer can inhibit the swelling deformation of ES layer both by deadweight and ion migration during the saturation process.

Acknowledgments

This work was supported by the National Natural Science Foundation of China (42077262, 42077261 and 41972294).

References

AbuHassanein, Z.S., Benson, C.H. and Blotz, L.R. (1996), "Electrical resistivity of compacted clays", *J. Geotech. Eng.-ASCE*, **122**(5), 397-406. https://doi.org/10.1061/(asce)0733-9410(1996)122:5(397).

Ali, M., Aziz, M., Hamza, M. and Madni, M.F. (2020), "Engineering properties of expansive soil treated with polypropylene fibers", *Geomech. Eng.*, **22**(3), 227-236. https://doi.org/10.12989/gae.2020.22.3.227.

Archie, G.E. (1942), "The electrical resistivity log as an aid in determining some reservoir characteristics", *Transactions, American Institute of Mining, Metallurgical and Petroleum Engineers*, **146**(1), 54-61. https://doi.org/10.2118/942054-G.

Bowels, J.E. (1988), *Foundation analysis and design*, McGraw-Hills Inc., USA.

Cai, G.H., Du, Y.J., Liu, S.Y. and Singh, D.N. (2015), "Physical properties, electrical resistivity, and strength characteristics of carbonated silty soil admixed with reactive magnesia", *Can. Geotech. J.*, **52**(11), 1699-1713. https://doi.org/10.1139/cgj-2015-0053.

Chen, S., Yu, S., Kong, L.W., Guo, A.G. and Liu, G. (2006), "Wrapping method for middle expansive soil embankment and its experimental verification", *Chinese J. Rock Mech. Eng.*, **25**(9), 1777-1783.

Cheng, Y., Wang, S., Li, J., Huang, X., Li, C. and Wu, J. (2018), "Engineering and mineralogical properties of stabilized expansive soil compositing lime and natural pozzolans", *Constr. Build. Mater.*, **187**, 1031-1038. https://doi.org/10.1016/j.conbuildmat.2018.08.061.

Chompoorat, T., Likitlersuang, S., Sitthiawiruth, S., Komolvilas, V., Jamsawang, P. and Jongpradist, P. (2021), "Mechanical properties and microstructures of stabilised dredged expansive soil from coal mine", *Geomech. Eng.*, **25**(2), 143-157. https://doi.org/10.12989/gae.2021.25.2.143.

Chu, Y., Liu, S. Y., Bate, B. and Xu, L. (2018), "Evaluation on expansive performance of the expansive soil using electrical responses", *J. Appl. Geophys.*, **148**, 265-271. https://doi.org/10.1016/j.jappgeo.2017.12.001.

Jones, L.D. and Jefferson, I. (2012), *Expansive soils*, Inst. of Civ. Eng, London.

Katti, R.K. (1979), *Search for Solutions to Problems in Black Cotton Soils*, First Indian Geotechn. Soc. Annu. Lect., Indian Geotechn. J., 9(1), 1-88.

Katti, R.K., Katti, A.R. and Katti, D.R. (2002), *Behaviour of Saturated Expansive Soil and Control Methods*, CBIP, Oxford &IBH, New Delhi.

Kibria, G. and Hossain, M.S. (2012), "Investigation of geotechnical parameters affecting electrical resistivity of compacted clays", *J. Geotech.Geoenviron. Eng.*, **138**(12), 1520-1529. https://doi.org/10.1061/(asce)gt.1943-5606.0000722.

Lei, J., Chen, W., Li, F., Yu, H., Ma, Y. and Tian, Y. (2021), "Investigation on moisture migration of unsaturated clay using cross-borehole electrical resistivity tomography technique." *Geomech. Eng.*, **25**(4), 295-302. https://doi.org/10.12989/gae.2021.25.4.295.

Murty, V.R. and Praveen, G.V. (2008), "Use of chemically stabilized soil as cushion material below light weight structures founded on expansive soils", *J. Mater. Civil Eng.*, **20**(5), 392-400. https://doi.org/10.1061/(ASCE)0899-1561(2008)20:5(392).

Nalbantoğlu, Z. (2004), "Effectiveness of class C fly ash as an expansive soil stabilizer", *Constr. Build. Mater.*, **18**(6), 377-381. https://doi.org/10.1016/j.conbuildmat.2004.03.011.

Oh, T.M., Cho, G.C., Son, T.A., Ryu, H.H. and Lee, C. (2015), "Experimental approach to evaluate weathering condition of granite using electrical resistivity", *Geomech. Eng.*, **8**(5), 675-685. https://doi.org/10.12989/gae.2015.8.5.675.

Punthutaecha, K., Puppala, A.J., Vanapalli, S.K. and Inyang, H. (2006), "Volume change behaviors of expansive soils stabilized with recycled ashes and fibers", *J. Mater. Civil Eng.*, **18**(2), 295-306. https://doi.org/10.1061/(asce)0899-1561(2006)18:2(295).

Puppala, A.J., Intharasombat, N. and Vempati, R.K. (2005), "Experimental Studies on Ettringite-Induced Heaving in Soils", *J. Geotech. Geoenviron. Eng.*, **131**(3), 325-337. https://doi.org/10.1061/(asce)1090-0241(2005)131:3(325).

S9451 (1994), "Guidelines for lining of canals in expansive soils (Second revision)", *Indian Standard*.

Watanabe, K., Nakajima, S., Fujiwara, T., Yoshii, K. and Venkatappa Rao, G. (2021), "Construction and field measurement of high-speed railway test embankment built on Indian expansive soil "Black Cotton Soil", *Soils Found.*, **61**(1), 218-238. https://doi.org/10.1016/j.sandf.2020.08.008.

Yao, H.L., She, J.B., Lu, Z., Luo, X.W., Xian, S.H., Fang, R. and Chen, Z.Z. (2020), "Inhibition effect of swelling characteristics of expansive soil using cohesive non-swelling soil layer under unidirectional seepage", *J. Rock Mech. Geotech. Eng.*, **12**(1), 188-196. https://doi.org/10.1016/j.jrmge.2019.07.008.

CG